POLYPUBLIE
Polytechnique Montréal

POLYTECHNIQUE MONTRÉAL
UNIVERSITÉ D'INGÉNIERIE

Titre: Development of a renewable technology for air heating and thermal cooling of sub-arctic mines using spray freezing
Title:

Auteurs: Mohammaderfan Mohit, Saad Akhtar, Minghan Xu, & Agus P. Sasmito
Authors:

Date: 2025

Type: Article de revue / Article

Référence: Mohit, M., Akhtar, S., Xu, M., & Sasmito, A. P. (2025). Development of a renewable technology for air heating and thermal cooling of sub-arctic mines using spray freezing. International Journal of Thermal Sciences, 211, 109704 (13 pages). https://doi.org/10.1016/j.ijthermalsci.2025.109704
Citation:

Document en libre accès dans PolyPublie
Open Access document in PolyPublie

URL de PolyPublie: https://publications.polymtl.ca/62777/
PolyPublie URL:

Version: Version officielle de l'éditeur / Published version
Révisé par les pairs / Refereed

Conditions d'utilisation: Creative Commons Attribution-Utilisation non commerciale-Pas d'oeuvre dérivée 4.0 International / Creative Commons Attribution-NonCommercial-NoDerivatives 4.0 International (CC BY-NC-ND)
Terms of Use:

Document publié chez l'éditeur officiel
Document issued by the official publisher

Titre de la revue: International Journal of Thermal Sciences (vol. 211)
Journal Title:

Maison d'édition: Elsevier
Publisher:

URL officiel: https://doi.org/10.1016/j.ijthermalsci.2025.109704
Official URL:

Mention légale: © 2025 The Author(s). Published by Elsevier Masson SAS. This is an open access article under the CC BY-NC-ND license (http://creativecommons.org/licenses/by-nc-nd/4.0/)
Legal notice:

Ce fichier a été téléchargé à partir de PolyPublie, le dépôt institutionnel de Polytechnique Montréal
This file has been downloaded from PolyPublie, the institutional repository of Polytechnique Montréal

https://publications.polymtl.ca

International Journal of Thermal Sciences 211 (2025) 109704

Contents lists available at ScienceDirect

International Journal of Thermal Sciences

journal homepage: www.elsevier.com/locate/ijts

Development of a renewable technology for air heating and thermal cooling of sub-arctic mines using spray freezing

Mohammaderfan Mohit [a,1], Saad Akhtar [a,b,1], Minghan Xu [a], Agus P. Sasmito [a,*]

[a] Department of Mining and Materials Engineering, McGill University, Montreal, QC H3A0E8, Canada
[b] GERAD and Department of Mathematics and Industrial Engineering, Polytechnique Montreal, Montreal, QC H3T1N8, Canada

ARTICLE INFO

Keywords:
Renewable heating and cooling
Mine ventilation
Spray freezing
Droplet solidification
Monte Carlo method

ABSTRACT

Mining industry is associated with high energy consumption and greenhouse gas (GHG) emissions due to intensive extraction processes and reliance on fossil fuel, specifically propane and diesel. In remote mines located in sub-arctic climates, heating and cooling operations can take up to half of this energy consumption, highlighting the importance of exploring innovative clean alternatives. The present study investigates one emerging solution to address this energy demand, known as spray freezing, in which the solidification of water droplets is used to provide the heating and cooling needs of mines. A multiscale thermo-hydraulic framework for spray freezing is developed, coupling the multi-stage droplet solidification process with a reduced-order spray-droplet dynamics model. Parametric studies are conducted using the Monte-Carlo method to quantify the effects of operating parameters on the system performance. It is found that the heat rate and cooling capacity of the spray freezing system are predominantly influenced by water flow rate and air temperature. Increasing the water flow rate from 7.5 kg/s to 30 kg/s can increase the heat rate to up to 400%. The ice generation of the system depends most on the air temperature, increasing significantly when the temperature drops below the water nucleation point, approximately -14 °C. Eventually, a multi-variate regression method is used to derive three user-friendly correlations that predict the heat rate, outlet air temperature, and ice generation of the spray freezing system, allowing a quick evaluation of the system performance in on-site applications.

1. Introduction

Providing heating and cooling demands of mines consumes a remarkable amount of energy, resulting in high operating costs [1]. For ventilation purposes, air flow rates in the order of 500 kilo cubic feet per minute (kCFM) to 2 million cubic feet per minute (MCFM) should be heated up to comfort temperatures of around 2 °C to avoid infrastructure freezing and provide a suitable working environment for miners. The energy-intensity of ventilation plants increases significantly when it comes to mines located in sub-arctic areas, such as northern Québec. Heating up 1 MCFM of air from sub-arctic temperature of −20 °C to 2 °C requires a significant power of 14 MW. For extreme conditions, the power consumption will rise to as much as 65 MW for heating 2 MCFM of air from −50 °C to 2 °C. The required power is generally provided through the use of fossil fuels, specifically propane and diesel, which are highly pollutant and expensive. Consequently, the annual heating costs for a typical mine in Northern Canada can reach up to CAD 8 million. [2,3]. The mentioned challenges are not limited to the heating case only, as the air cooling is also essential during the mine operations, particularly for deep and ultra-deep mines (depth of more than 1.5 km). In these mines, efficient air cooling systems are necessary to suppress the auto-compression effects and remove the heat emitted from equipment and surrounding rocks [4]. For example, an ultra-deep mine in northern Québec installed 11.6 MW of surface refrigeration plant, 4.2 MW of underground refrigeration plant at shallow level, and 21 MW of refrigeration plant at deeper levels (in total around 36.8 MW of refrigeration systems) [5,6]. Overall, a heating and cooling system for underground mines can cost as high as CAD 50M in capital investment [7]. Therefore, development of renewable technologies to provide the energy demand of mines has never been more critical than in the present day [8].

One solution to address the energy demand in mine operations is called spray freezing, in which the release of latent heat during the solidification of water is utilized to heat up air. This technology involves atomizing water through nozzles and injecting it onto an air

* Corresponding author.
E-mail address: agus.sasmito@mcgill.ca (A.P. Sasmito).
[1] These authors contributed equally to this work.

https://doi.org/10.1016/j.ijthermalsci.2025.109704
Received 16 October 2024; Received in revised form 8 January 2025; Accepted 10 January 2025
Available online 24 January 2025
1290-0729/© 2025 The Author(s). Published by Elsevier Masson SAS. This is an open access article under the CC BY-NC-ND license (http://creativecommons.org/licenses/by-nc-nd/4.0/).

Nomenclature

A	Surface area (m^2)
c_p	Specific heat capacity (J kg^{-1} K^{-1})
C_D	Drag coefficient
d	Diameter (m)
e	Energy (J)
g	Gravitational acceleration (m s^{-2})
h_{eq}	Equivalent heat transfer coefficient (W m^{-2} K^{-1})
J	Nucleation rate (m^{-3} s^{-1})
k	Thermal conductivity (W m^{-1} K^{-1})
k_B	Boltzmann constant (m^2 kg^{-1} s^{-2} K^{-1})
L_{eff}	Effective latent heat of fusion (J kg^{-1})
M	Molecular weight (kg $mole^{-1}$)
m	Mass (kg)
N_A	Avogadro's constant (mol^{-1})
N_v	Number of nuclei formed
P	Pressure (Pa)
p	Probability
Q	Cumulative distribution
Q_h	Heat rate (MW)
r	Radius (m)
T	Temperature (K)
t	Time (s)
T_∞	Ambient air temperature (K)
u	Velocity (m s^{-1})
V	Volume (m^3)
x	Position (m)

Abbreviations

CFD	Computational fluid dynamics
IPF	Ice packing fraction
PDE	Partial differential equation
SMD	Sauter mean diameter

Greek symbols

α	Thermal diffusivity (m^2 s^{-1})
μ	Dynamic viscosity (Pa s)
ρ	Density (kg m^{-3})
σ	Surface tension (N m^{-1})
τ	Dimensionless time

Superscripts and subscripts

a	Air
c	Crystal
eq	Equivalent
f	Freezing
homo	Homogeneous
init	Initial
i	Interface
l	Liquid
nuc	Nucleation
op	Operation
p	Droplet
rec	Recalescence
spc	Supercooling
s	Solid

stream whose initial temperature is below the water freezing point [9]. The release of latent heat from water to air causes the air temperature to rise and water droplets to freeze, resulting in the formation of ice pieces. The produced ice particles are either accumulated to be used during summer or continuously pumped into the cooling units. This method has shown promising performance for mine heating and cooling when used in sub-arctic climates [10]. However, the efficient field-scale implementation of this setup requires further development through theoretical and experimental studies. Particularly, a better understanding of the freezing and dynamics of water droplets needs to be developed in the context of spray freezing. Droplet freezing has received much attention in the literature due to its extensive applications in nature and industry [11]. Researchers conducted various experimental and theoretical studies to analyze this process [12,13]. From theoretical point of view, some researchers employed the Stefan formulation to represent the droplet freezing process. The Stefan problem is a general term for a set of moving boundary problems, where a set of partial differential equations (PDEs) are solved simultaneously, one of which represents the moving boundary (known as the Stefan condition) [14,15]. Analytical solutions to the Stefan problem are developed under specific conditions using the perturbation series solution along with the asymptotic analysis [16]. Additionally, experimental studies concerning the freezing of suspended [17] and sessile [18] droplets were reported, capturing the freezing stages and the droplet temperature profile. While the outlined studies provide a solid understanding of the droplet freezing process, there is a gap in the literature regarding the study of droplet solidification in the context of spray freezing, particularly considering the coupling of freezing and droplet dynamics.

Studying the dynamic behavior of moving droplets, bubbles, and solid particles inside fluid flows is generally categorized under the two-phase flows' literature [19,20]. The equation of motion can predict the velocity profile and trajectory of a moving droplet within a spray [21]. Several scholars employed numerical approaches to solve the equation of motion to capture dynamics of droplets [22,23]. To model the dynamics of spray freezing, studying the spray characteristics, including its angle, type, and size distribution is of primary importance as well [24]. Although droplet freezing and dynamics phenomena were extensively studied in the literature separately, few efforts have been carried out to couple both phenomena to model the spray freezing system. A review on the modeling of spray freezing system and related research gaps can be found in [25]. Anandharamakrishnan et al. [26] introduced a computational fluid dynamics (CFD) model for spray freezing, encompassing both the dynamics and solidification of droplets. However, their model is computationally expensive and lacks enough resolution in the droplet freezing process, as it neglects the nucleation and crystal growth processes. Hindmarsh et al. [27] studied the freezing of a suspended droplet; however, their framework was limited to a single droplet and was not extended to the spray scale. Sebastiao et al. [28] developed a kinetic model for spray freezing in pharmaceuticals, but their model requires high computational power and does not consider the air flow model in the spray dynamics. Furthermore, they did not compute system-level thermal performance of spray freezing setup and the impact of various parameters on the system thermodynamics, including the air temperature and flow rate, nozzle properties, and water flow rate, among others.

Considering the mentioned studies, the following research gaps are identified:

1. Existing models of spray freezing are associated with a low resolution in the freezing model, ignoring the nucleation and recalescence stages, and high computational cost in the dynamics model.
2. The effects of air flow in the hydrodynamic model of spray-droplet have not been quantified in the previous studies related to the spray freezing.

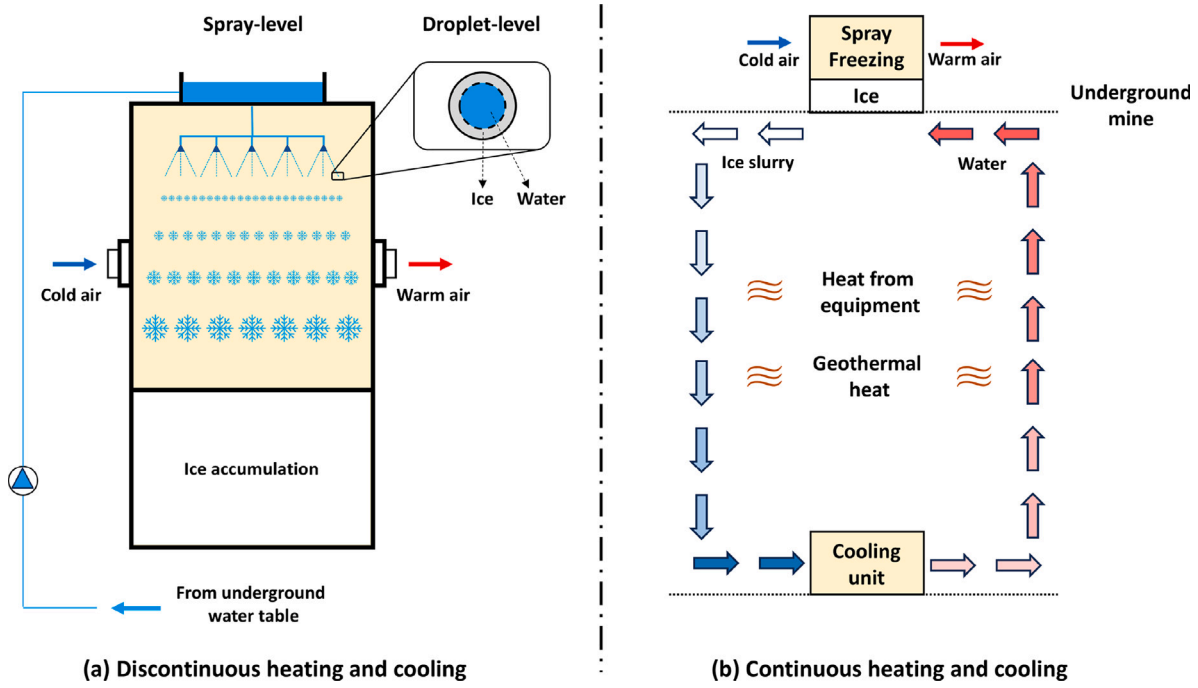

Fig. 1. Schematic diagram of the spray freezing: (a) Discontinuous heating and cooling highlighting different physical scales (b) Continuous heating and cooling.

3. The influence of operating parameters on spray freezing performance has not been thoroughly studied, leaving limited insight for the optimal design of the system.

Considering the mentioned research gaps, this study, first, outlines a fast-to-compute thermo-hydraulic framework for spray freezing by combining models of droplet freezing, spray-droplet dynamics, and air flow. The droplet freezing model, capable of capturing the solidification process at different time and length scales, is coupled with a reduced-order model of spray-droplet dynamics that takes into account the air flow. The developed model is validated against field-scale data gathered from the Frood-Stobie mine [10]. Consequently, the heat rate, cooling capacity, outlet air temperature, and ice generation of the setup are computed using the developed model. A parametric study is conducted using the Monte-Carlo method to analyze the effects of various operating parameters, including spray pressure, water flow rate, and air flow rate and temperature on the overall system outputs. Lastly, a multi-variate regression analysis is employed to formulate three fast-to-compute correlations for predicting the heat rate, outlet air temperature, and ice generation of spray freezing setup for on-site applications.

The rest of the paper is organized as follows. In Section 2, the methodology and mathematical modeling are introduced and validated against the experimental data. Section 3 involves representing the results, including the Monte-Carlo study and regression analysis. Concluding remarks and avenues of future work are identified in Section 4.

2. Methodology

The schematic of the spray freezing setup is shown in Fig. 1. Two configurations can be considered for the system, including the continuous and discontinuous heating and cooling. As illustrated in Fig. 1(a), the discontinuous heating and cooling involves drawing water from underground sources and spraying it into the incoming cold air stream inside a stope. The release of latent heat during heat transfer between the droplets and air causes the droplets to freeze and raises the air temperature, the latter is an alternative way to heat up air instead of using fossil fuels. The frozen droplets are accumulated at the bottom of the chamber in the form of ice packs or slurries, which can be later used for cooling purposes. This setup was successfully implemented in the Frood-Stobie mine in Sudbury Basin, Ontario [10], and is capable to provide the required heating of 650 kCFM of air. It also produces an approximate amount of 145,000 tons of ice during the winter operations, which is stored to be used for cooling in the summer.

Fig. 1(b) shows the continuous heating and cooling scenario. In this case, the ice slurries generated during the spray freezing are continuously pumped into a cooling unit, where the slurries absorb heat and turn into the water. The liquid water is then returned to the spray freezing setup to complete the cycle. Kidd mine in Timmins, Ontario [7] is a practical example of this continuous cooling configuration. The typical method to provide the heating and cooling needs of mines is to burn fossil fuels such as propane and diesel. Trapani [29] conducted a techno-economic study on the heating and cooling methods for mines and showed that the cost per unit of energy is approximately $70/MWh and $80/MWh for spray freezing and conventional system, respectively. Thus, spray freezing offers a cleaner and less expensive solution for mine ventilation compared to traditional methods. The potential of the latent heat of water during the phase change process to heat up air highlights the significance of developing a precise mathematical framework for spray freezing to predict the system-level thermal performance while incorporating droplet-level phenomena. These two scales — droplet-level and spray-level — are also conceptually illustrated in Fig. 1(a).

The theoretical model consists of two sub-models, including droplet freezing and spray-droplet dynamics. The freezing model involves a semi-analytical, five-stage model of droplet solidification. In the spray-droplet dynamics model, the distributions of droplets' dynamical characteristics, including, trajectory, velocity, and residence time are predicted. The 3D air flow is incorporated into the model using ANSYS Fluent software package. In the following sections, these sub-models are introduced. Consequently, the parametric studies and regression analysis are discussed.

2.1. Droplet freezing model

The freezing of droplets consists of five distinct stages. Initially, the temperature of the droplet drops below its freezing point, in a

stage known as liquid supercooling. Consequently, minuscule ice embryos begin to form inside the droplet—a process called nucleation. Following nucleation, the surrounding supercooled molecules attach to these nuclei, forming a crystalline structure within the droplet. This crystallization is accompanied by the release of latent heat, causing the droplet's temperature to rise back to the freezing point (crystal growth or recalescence stage). Subsequently, the solid phase begins to form from the outer surface of the droplet in a stage called equilibrium freezing. Once equilibrium freezing is complete, the resulting solid particles continue to exchange heat with the environment until they reach thermal equilibrium, a process referred to as solid subcooling. In this paper, a unified multiscale model for droplet freezing is formulated, capable of predicting the five stages of the droplet solidification. The following assumptions are made for this unified phase change model:

1. Heat conduction is the dominant mode of heat transfer. Heat convection and radiation are not modeled by the governing equation, but they are incorporated into the heat transfer coefficient at the outer boundary.
2. One-dimensional heat conduction in the droplet is assumed.
3. The contribution of latent heat during freezing is much higher than that of sensible heat (i.e., a low Stefan number); therefore, only the solid phase affects the interfacial motion.
4. Thermophysical properties depend on the phase rather than the specific temperature.
5. The volume change of the droplet during solidification is neglected.
6. The crystal velocity is assumed to be constant during the recalescence stage.

Formulation. The unified model is governed by a one-dimensional transient heat equation with a source term

$$\frac{1}{\alpha}\frac{\partial T}{\partial t} = \frac{\partial^2 T}{\partial r^2} + \frac{2}{r}\frac{\partial T}{\partial r} + \frac{g_0}{k}, \quad 0 < r < r_p, \quad t > 0, \tag{1}$$

where $\alpha, T, t, r, g_0, k, r_p$ are the thermal diffusivity, droplet temperature, time, r-coordinate, internal heat generation, thermal conductivity, and droplet radius, respectively. Two fixed boundary conditions are prescribed at the center and the outer surface of the droplet as follows

$$\begin{aligned} &T(r \to 0, t) \Rightarrow \text{finite}, \\ &-k\frac{\partial T}{\partial r}\bigg|_{r=r_p} = h_{eq}\Big[T(r = r_p, t) - T_\infty\Big], \end{aligned} \tag{2}$$

where h_{eq} and T_∞ are the equivalent heat transfer coefficient and ambient air temperature, respectively. In addition, a moving boundary condition is also imposed when the solid and liquid phases coexist at the equilibrium freezing stage (also known as the Stefan condition)

$$\begin{aligned} &k_s\frac{\partial T_s}{\partial r}\bigg|_{r=r_i(t)} = \rho_s L_{eff}\frac{dr_i}{dt}, \\ &T(r = r_i(t), t) = T_f, \end{aligned} \tag{3}$$

where $r_i(t), \rho, L_{eff}, T_f$ are the solid–liquid interface location, mass density, effective latent heat, and fusion temperature, respectively. The subscript "s" represents the solid phase, and "l" will stand for the liquid. Moreover, the time conditions for T and r_i are given by

$$\begin{aligned} T_l(r, t = 0) &= T_{init}, \\ T_l(r, t = t_{nuc}) &= T_{nuc}, \\ T_s(r, t_{rec}) &= T_f, \\ r_i(t = t_{rec}) &= r_p, \\ r_i(t = t_f) &= 0, \end{aligned} \tag{4}$$

where subscripts "init", "nuc", "rec", "f" show the initial, nucleation, recalescence (or crystal growth), and (equilibrium) freezing states, respectively. Moreover, the source term is a piece-wise function that switches on during the recalescence stage only

$$g_0 = \begin{cases} \dfrac{\rho c_p \Delta T_{spc}}{\Delta t_{rec}} & \text{if } t_{nuc} \le t \le t_{rec} \\ 0 & \text{otherwise,} \end{cases} \tag{5}$$

where ΔT_{spc} is the supercooling degree, and Δt_{rec} is the time duration of crystal growth given by $\Delta t_{rec} = t_{rec} - t_{nuc}$. It is noted that this unified model is a revised version of our previous work [30], where a two-dimensional cylinder was considered for inward solidification of PCMs.

Table 1
Analytical solution for the liquid supercooling stage.

Formula	Description
$\frac{T_l - T_\infty}{T_{init} - T_\infty} = \sum_{n=1}^{\infty} \frac{2(\sin\beta_n - \beta_n\cos\beta_n)}{\beta_n - \sin\beta_n\cos\beta_n} \frac{\sin(\beta_n r/r_p)}{\beta_n r/r_p} \exp\left(-\frac{\beta_n^2 \alpha_l}{r_p^2} t\right)$	Series solution
$\beta_n \cos\beta_n + (\mathrm{Bi}_l - 1)\sin\beta_n = 0$	Eigenvalues
$\mathrm{Bi}_l = h_{eq} r_p / k_l$	Biot number

Methods and solutions. In the first stage (liquid supercooling), the unified model reduces to a transient heat conduction problem subjected to a convective boundary condition without any phase change (i.e., source term). An exact solution of the liquid temperature profile T_l can be found using the separation of variables as expressed in Table 1.

Using the temperature profile calculated from the heat equation and corresponding boundary conditions, the nucleation rate for a supercooled droplet can be computed. The dominant mechanism for nucleation is the heterogeneous nucleation, in which the new phase is formed on the surface of a foreign material. The heterogeneous nucleation rate can be calculated using the following expression derived from the Classical Nucleation Theory (CNT)

$$J = \frac{N_A \rho_l}{M_l} Z_{het} f \exp\left(-\frac{\Phi \Delta G^*}{k_B T_l}\right), \tag{6}$$

where N_A, ρ_l, M_l, f, k_B, and T_l are the Avogadro's constant, water density, water molecular weight, net rate of attachment to the critical nucleus, Boltzmann constant, and the supercooled droplet temperature, respectively. Parameter Z_{het} is the heterogeneous Zeldovic factor, representing the probability of a nucleus to grow and remain stable. The rate of heterogeneous nucleation is controlled by the critical free energy barrier, $\Phi\Delta G^*$. Using the nucleation rate expression, we can calculate the probability of nuclei formation in the supercooled droplet as a function of time. Physically, when the temperature of the droplet falls below the freezing point, it starts approaching the thermodynamic free energy barrier. This implies that the probability of forming an ice embryo inside the droplet starts increasing. The number of ice nuclei formed as a function of nucleation rate is given by the following integral

$$N_v = \int_0^t [V_0 - V_c(\tilde{t})] J(\tilde{t}) d\tilde{t}. \tag{7}$$

Here, N_v is the number of nuclei formed, $V_c(t)$ is the volume of the ice crystal, V_0 is the initial droplet volume, and $J(t)$ is the nucleation rate. The time and temperature at which N_v reaches 1 are recorded as the nucleation time and nucleation temperature, respectively.

Following nucleation, the crystallization stage takes place over a short timescale. A modified Wilson–Frenkel model is employed to model this stage, incorporating the curvature under-cooling, kinetic, and thermal effects [31]. The recalescence time, Δt_{rec}, can be computed from the growth velocity, v. The internal heat generation g_0 is therefore calculated by the ratio of the supercooling degree over the recalescence time, i.e., $g_0 = \rho c_p \Delta T_{supercool}/\Delta t_{rec}$, as given by [30]. An exact solution can also be obtained in this case with a constant source term by employing the superposition rule to find the non-homogeneous term. Let the right-hand side of the series solution given Table 1 be the homogeneous part θ_{homo} of this solution, and then the solution to the

Table 2
Formulation of the equilibrium freezing stage.

Formula	Description
$\frac{1}{\alpha_s}\frac{\partial T_s}{\partial t} = \frac{\partial^2 T_s}{\partial r^2} + \frac{2}{r}\frac{\partial T_s}{\partial r}$	Governing equation for Stefan problem
$k_s \frac{\partial T_s}{\partial r}\Big\|_{r=r_i(t)} = \rho_s L_{\text{eff}} \frac{dr_i}{dt}$	Stefan condition
$-k_s \frac{\partial T_s}{\partial r}\Big\|_{r=a} = h_{\text{eq}}\left[T_s(r=a,t) - T_\infty\right]$	Boundary condition 1
$T_s(r=r_i,t) = T_f$	Boundary condition 2
$T_s(r,t=0) = T_f$	Time condition 1
$r_i(t=0) = a$	Time condition 2
$r_i(t=t_f) = 0$	Time condition 3

liquid phase is expressed as

$$\frac{T_l - T_\infty}{T_{\text{init}} - T_\infty} = \theta_{\text{homo}} + \frac{g_0}{3\text{Bi}_l} + \frac{g_0}{6}\left[1 - \frac{r^2}{r_p^2}\right]. \tag{8}$$

After the crystal growth stage, the temperature of the droplet rises to the equilibrium point, initiating the phase change process in a stage known as the equilibrium freezing stage. The effective latent heat can be computed as

$$L_{\text{eff}} = \left(1 - \frac{c_{p,l}}{c_{p,s}}\text{Ste}_s\right)L, \tag{9}$$

where L is the water latent heat of fusion. The equilibrium freezing stage can be formulated as a one-phase Stefan problem. The governing equation and boundary conditions are given in Table 2, in which t_f is the total time of the equilibrium freezing stage.

The solution to the Stefan problem outlined in Table 2 can be obtained by non-dimensionalizing the parameters as follows

$$\Theta_s = \frac{T_s - T_\infty}{T_f - T_\infty}, \qquad \eta = \frac{r}{a}, \qquad \eta_i = \frac{r_i}{a},$$
$$\tau = \frac{\alpha_s t \text{Ste}}{a^2}, \qquad \text{Ste} = \frac{c_{p,s}(T_f - T_\infty)}{L_{\text{eff}}}, \qquad \text{Bi} = \frac{ha}{k_s}. \tag{10}$$

As discussed in [32], the outlined set of PDEs and boundary conditions can be solved using a series solution. The solution of the interface motion and temperature field can then be used to find the total solidification time in non-dimensional form as

$$\tau_f \sim \frac{2 + \text{Bi}_s}{6\text{Bi}_s}\left(1 + \text{Ste}_s\right), \tag{11}$$

where τ_f is the dimensionless freezing time given by $\tau_f = \frac{\alpha_s t_f}{r_p^2}$. After the equilibrium freezing, the fully frozen particle continues to transfer heat to the surrounding medium through conduction. The analytical solution for this solid subcooling stage is found in the same way as a liquid supercooling stage, except for a different initial condition and thermophysical properties specified for the solid phase.

As demonstrated by experimental studies [11,17], droplet freezing can occur without a supercooling phase, depending on the ambient temperature. If the ambient temperature is higher than the nucleation temperature, freezing will occur directly, bypassing supercooling. However, if the ambient temperature is lower than the nucleation temperature, the supercooling stage is triggered and must be accounted for. Fig. 2 showcases the two freezing scenarios predicted by the model for various droplet diameters. From Fig. 2(a), it is observed that when $T_\infty = -20$ °C, the supercooling stage occurs. However, for $T_\infty = -5$ °C, the freezing happens without supercooling process, as shown by Fig. 2(b).

2.2. Spray-droplet dynamics model

The heat emitted from droplets depends on their residence time — the time that a droplet remains within the system domain to transfer heat to the surrounding air — and relative velocity with air. Thus, it is essential to model the spray-droplet dynamics and couple it with the freezing model. The model developed here is solving the equation of motion — which relates the forces acting on the droplet to its velocity — for droplets individually to calculate their residence time and velocity. The air flow is separately modeled using the computational fluid dynamics (CFD) simulations, neglecting the effects of droplets on the flow field. Statistical distributions are then used to represent the size distribution of the spray, subsequently computing the velocity and residence time distributions of the spray. The drag and gravity are the primary forces acting on a moving droplet, thus the equation of motion can be formulated as given in Table 3.

Table 3
Formulation of droplet dynamics model.

Formula	Description
$\frac{du_p}{dt} = \frac{3\mu_a}{16r_p^2\rho_p} C_D \text{Re}_p (u_a - u_p) + g$	Equation of motion
$u_p = \frac{dx_p}{dt}$	Velocity of the droplet
$\text{Re}_p = \frac{\rho_a \lvert u_a - u_p \rvert d_p}{\mu_a}$	Reynolds number
$C_D = \begin{cases} (\frac{24}{\text{Re}_p})(1 + 0.15\text{Re}_p^{0.687}) & \text{Re}_p < 1000 \\ 0.44 & \text{Re}_p \geq 1000 \end{cases}$	Drag coefficient

In Table 3, x_p and u_p indicate the droplet position and velocity, respectively, μ_a is the air dynamic viscosity, r_p is the droplet radius, ρ_p and ρ_a are the droplet and air densities, respectively, and $d_p = 2r_p$ is the droplet diameter. This set of equations are numerically solved to calculate the droplet velocity at each time step, and then the droplet velocity is integrated over time to specify the droplet position. The residence time, τ_{rt}, of a droplet is then calculated by adding time steps until the droplet collides with the system boundaries. It can be seen from the formulation outlined by Table 3 that the air flow affects the dynamics of droplets and thus should be modeled carefully. We employed the CFD simulation via ANSYS Fluent v.18.1 to incorporate the air flow in the droplet dynamics model. The results for the Frood-Stobie mine are discussed here. In the Frood-Stobie mine, the air is delivered to the stope via a circular airway with a diameter of 6.1 m placed on the top of the stope and goes out through a similar airway placed on the side [10]. It is noted that while air velocity, u_a, is required in the droplet dynamics model, generally the air flow rate is given in practical applications. Hence, we conducted simulation studies to find the air velocity inside the mine stope for different air flow rates ranging from 400 kCFM to 2 MCFM. For the CFD simulation, we used a structured grid with refinements near the air entry and exit paths. The relatively simple geometry of the problem justified the use of structured grid. Compared to an unstructured grid, the regular arrangement of structured grids provides faster results with lower computational power and memory requirements. Also, by conducting mesh-independence studies and implementing mesh refinement, numerical accuracy and stability were ensured. The streamlines from the simulation for the minimum (400 kCFM) and maximum (2 MCFM) air flow rates are shown in Figs. 3(a) and (b), respectively. To incorporate the results into the droplet-scale models, the air flow is assumed to be a cross flow. As a result, the average air velocity in x-, y-, z-directions is calculated from the simulations and used in the droplet dynamics model.

The spray consists of hundreds of thousands of droplets with different diameters and velocities. To simplify our analysis, we assume that the droplet coalescence and breakup processes are negligible (i.e., a low Weber number). Also, the effect of droplet's deformation is ignored (i.e., a low Ohnesorge number). A conservation of energy can be used to find the total heat rate from water droplets to air

$$\dot{q}_t = \sum_{n=1}^{k} p_n \dot{N} e_n, \tag{12}$$

where p_n is the probability of the existence of a droplet with diameter "$d_{p,n}$", $\dot{N}$ is the particle injection rate, and e_n is the energy transfer

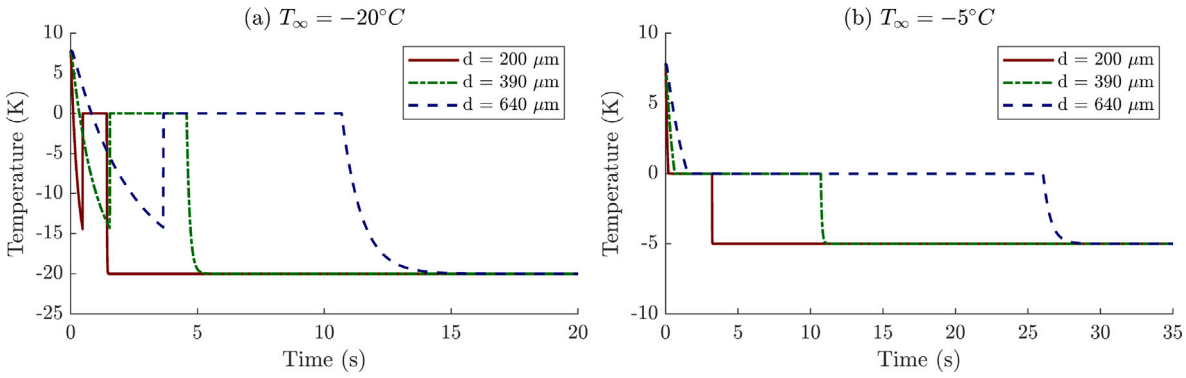

Fig. 2. The freezing curves of various droplets (a) With supercooling stage; (b) Without supercooling stage.

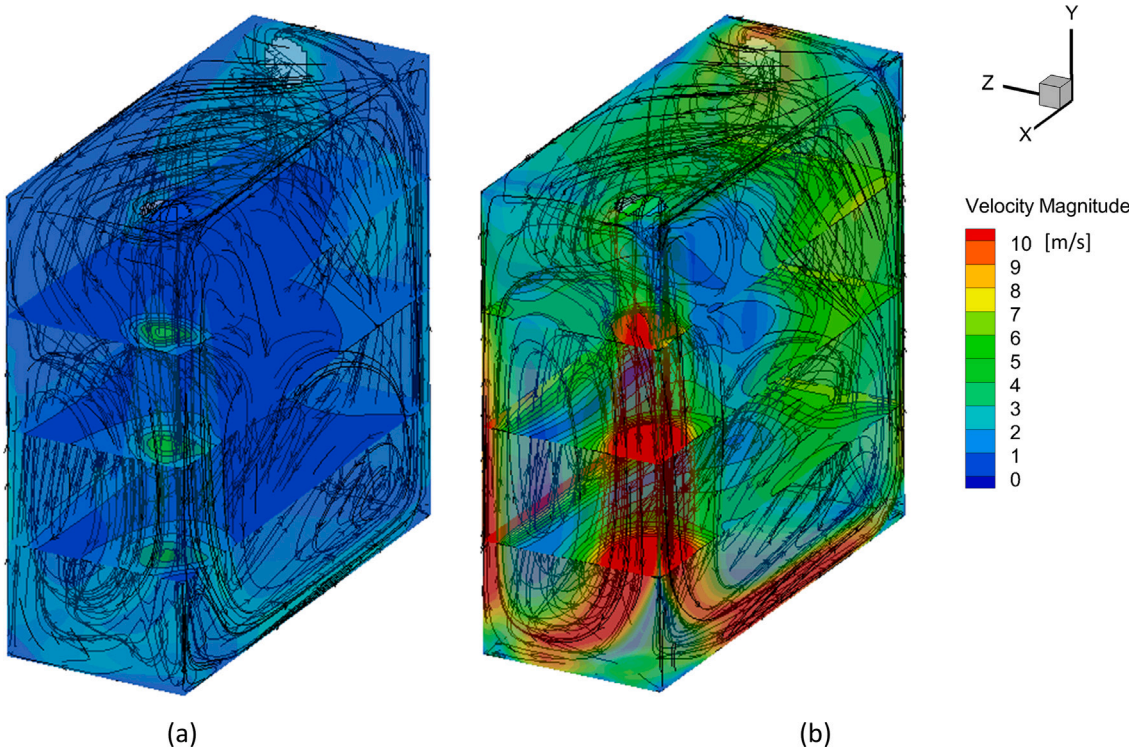

Fig. 3. Simulation results of the air flow streamlines for (a) Air flow rate of 400 kCFM (b) Air flow rate of 2 MCFM.

during the solidification of the droplet with size "$d_{p,n}$". Parameter $\dot{N}$ can be calculated using the conservation of mass principle

$$\dot{N} = \frac{\dot{m}_w}{\sum_{n=1}^{k} m_n p_n}, \tag{13}$$

where $\dot{m}_w$ is the total mass flow rate of the spray and $m_n = \frac{4}{3}\pi r_n^3 \rho_p$, is the mass of the droplet with radius r_n. In Eqs. (12) and (13), parameter k represents the number of different droplet sizes assumed for modeling. In our model $k = 20$, meaning that the droplet size distribution is discretized into 20 different sample sizes. The total energy transfer from a droplet can be calculated by integration

$$e_n = \int_0^{\tilde{t}} h_{eq,n} A_n (T_n(t) - T_\infty) dt, \tag{14}$$

where $T_n(t)$ is the temperature profile at the surface, A_n is the surface area, and $h_{eq,n}$ is the equivalent heat transfer coefficient for the nth droplet. The outlet temperature, $T_{a,out}$, is computed as

$$T_{a,out} = T_{a,init} + \frac{\Sigma e_n}{\dot{m}_a c_{p,a}}, \tag{15}$$

The ratio of the total frozen water (m_s) over the total amount of water injected into the system (m_w) is called the ice packing fraction (IPF)

$$\text{IPF} = \frac{m_s}{m_w} \times 100. \tag{16}$$

The IPF is calculated by integrating the frozen portion of all droplets within the system. To compute the frozen portion of each droplet, its residence time, τ_{rt}, is compared to its nucleation, τ_{nuc}, and freezing times, τ_f. It should be highlighted that the phase-dependency of the water density results in the volume change of droplets during the solidification process, which is neglected in the freezing model. To guarantee the mass conservation in spray-level, a mass correction term, ($\Delta m_{correction}$), is added in the IPF calculation. This parameter is computed by conserving the total mass of water injected into the system

$$\dot{m}_w = \sum_n p_n \dot{N} m_{s,n} + \sum_n p_n \dot{N} m_{l,n} + \Delta m_{correction}. \tag{17}$$

This term will be added to m_s when calculating IPF by Eq. (16).

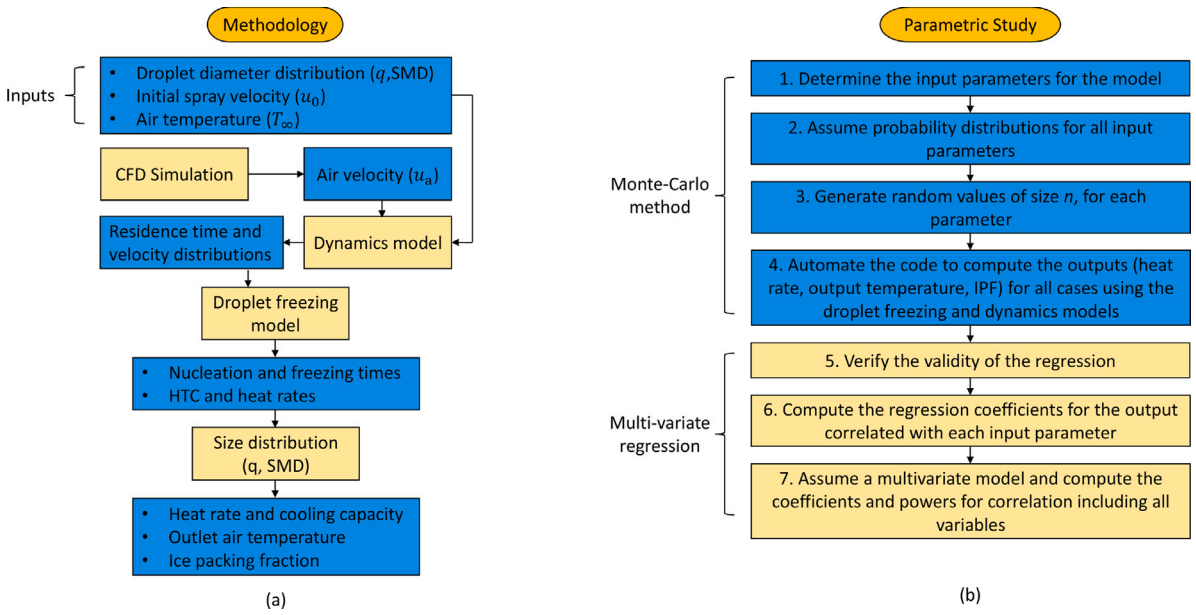

Fig. 4. Flowchart of the methodology: (a) Computation procedure of the model (b) Parametric study procedure.

The cooling capacity of the spray freezing setup can be calculated as

$$Q_c = \dot{m}_s \times L_{eff} \times t_{op} = \text{IPF} \times \dot{m}_w \times L_{eff} \times t_{op}, \tag{18}$$

where t_{op} is the total operating time.

The size distribution of droplets generated by a nozzle has significant effects on the overall performance of the spray freezing setup. This distribution depends on multiple factors, including nozzle pressure and flow rate, type of fluid being sprayed, and fluid temperature [33]. Various correlations have been reported in the literature to compute the size distribution of nozzles. The Rosin–Rammler distribution is one of the mostly used functions to represent the droplet size distribution [24]

$$Q(d) = 1 - \exp\left[-\Gamma\left(1 - \frac{1}{q}\right)^{-q}\left(\frac{d}{\text{SMD}}\right)^{q}\right], \tag{19}$$

where $Q(d)$ is the cumulative probability of the existence of a droplet with diameter d in the spray, SMD is the Sauter Mean Diameter, and q determines the tightness of the distribution. The SMD is defined as below

$$\text{SMD} = \frac{\Sigma N_i d_i^3}{\Sigma N_i d_i^2}, \tag{20}$$

where d_i is the droplet diameter and N_i is the number of droplets with diameter d_i. The spray freezing system of the Frood-Stobie mine utilizes a flat spray nozzle [10], for which the following correlation is proposed to calculate SMD [24]

$$\text{SMD} = 2.83 d_0 \left(\frac{\sigma \mu_l^2}{\rho_a d_0^3 \Delta P_l^2}\right)^{0.25} + 0.26 d_0 \left(\frac{\sigma \rho_l}{\rho_a d_0 \Delta P_l}\right)^{0.25}, \tag{21}$$

where d_0 is the nozzle diameter, ρ_a is the air density, σ, μ_l, and ρ_l are the surface tension, viscosity, and density of water, respectively, and ΔP_l is the spray pressure.

Fig. 4(a) demonstrates the computation procedure of the outlined framework. The following steps summarize the calculation process

1. Input parameters, including parameters of the diameter distribution (SMD and q), initial spray velocity (u_0), and air temperature (T_∞) are fed into the dynamics model,
2. The CFD simulation calculates the air velocity (u_a) to be used in the dynamics model,
3. From the dynamics model, the residence time and velocity distributions of droplets are calculated and fed into the freezing model,
4. The freezing model computes the nucleation and freezing times and heat rate of each droplet,
5. Using the size distribution, the system-level calculations are conducted.

Compared to existing results, the present model offers the following advantages:

1. The reduced-order dynamics model of droplets requires less computational power compared to CFD models, while maintaining acceptable precision.
2. Unlike existing models, the presented freezing model accounts for the nucleation and crystallization stages.
3. The influence of air flow on the dynamics model is considered.

It should be highlighted that in the present study, a one-way coupling method is used to model the interactions between droplets and the continuous phase, neglecting the effects of droplets on the continuous phase. This assumption reduces the computational load and is justified by the low droplet volume fraction in spray freezing systems used for mine ventilation. For example, in the Frood-Stobie mine, the droplet volume fraction is approximately 4%, indicating a minimal impact on the air phase.

2.3. Parametric studies and regression analysis

The efficiency of the spray freezing system to provide the heating and cooling requirements of mines can be represented in terms of the heat rate, cooling capacity, outlet air temperature, or ice packing fraction (IPF). It is imperative to conduct parametric studies to quantify the effects of operating parameters on these performance criteria. To develop correlations to calculate the output variables of interest as a function of input parameters, multi-variate regression method can be employed. The water flow rate, air flow rate, ambient temperature, and spray pressure are the input variables in the present study. To perform regression, an input–output dataset representing the physical system across various operating points should be generated. The Monte Carlo method has proven to be an efficient tool for systematically conducting parametric studies and analyzing the influence of input parameter variations on system performance. It involves repetitive simulations using randomly generated sets of input data to compute the output data space. The primary purpose of conducting a Monte

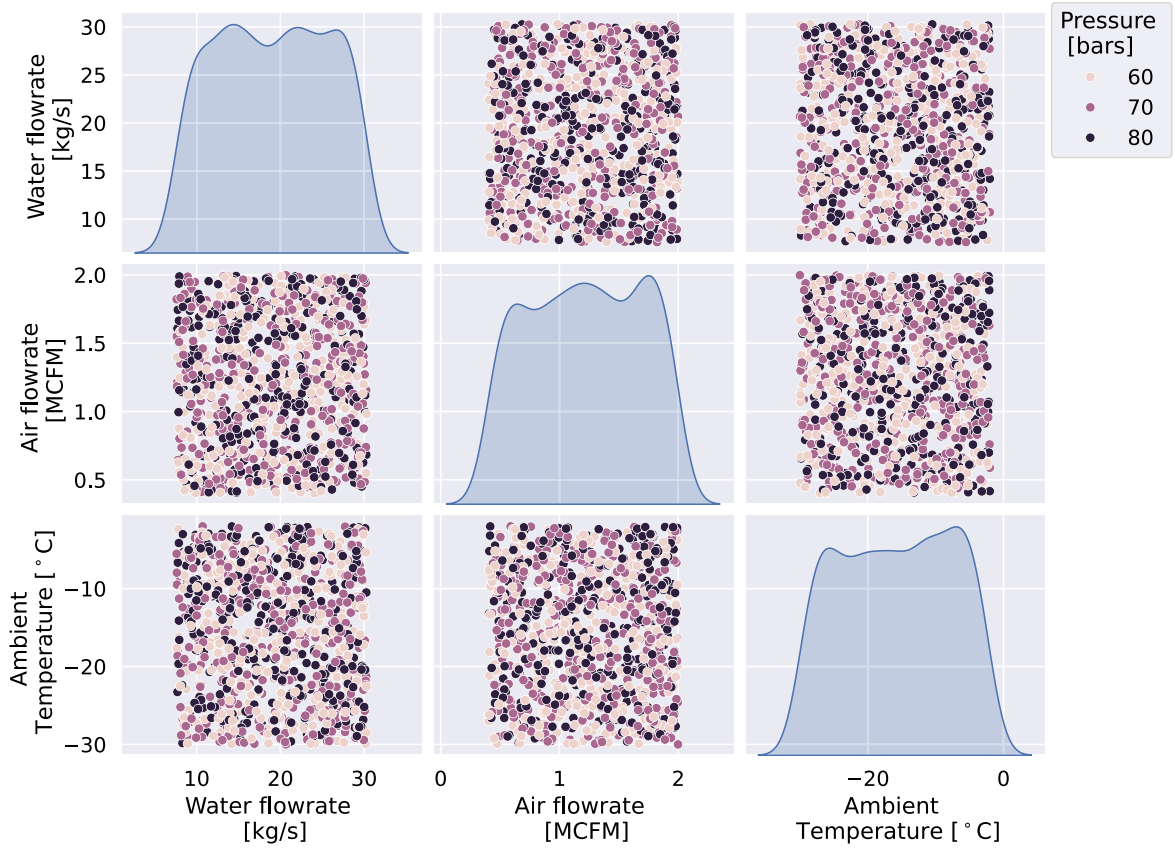

Fig. 5. Input parameter space for the parametric study of the spray freezing.

Table 4
The operating parameters and their corresponding ranges and distributions used in the parametric studies.

Parameter	Max	Average	Min	Distribution
Water flow rate [kg/s]	30.3	18.9	7.5	Uniform
Ambient temperature [K]	271	258	243	Normal
Air flow rate [CFM]	2,000,000	1,200,000	400,000	Uniform
Spray pressure [bar]	80	70	60	Uniform (Discrete)

Carlo study is to perform sensitivity analysis and quantify the effects of uncertainties in input parameters on output variables. The significance of the Monte Carlo method lies in its robustness and its capability to generate statistical insights into the system, rather than providing single-point information.

The outline of the methodology is demonstrated in Fig. 4(b). Four sample sizes, namely 100, 200, 500, and 1000 cases, have been tested to ensure the size-independence of the parametric study conducted via the Monte-Carlo method. A multi-variate regression analysis is performed to suggest correlations for the heat rate, outlet air temperature, and IPF as follows

$$\dot{Q}_{\mathrm{h}} = a_1 \dot{m}_{\mathrm{w}}^{p_{11}} + b_1 \dot{m}_{\mathrm{a}}^{p_{12}} + c_1 T_{\infty}^{p_{13}} + d_1 P_{\mathrm{spray}}^{p_{14}} + e_1, \tag{22a}$$

$$T_{\mathrm{a,out}} = a_2 \dot{m}_{\mathrm{w}}^{p_{21}} + b_2 \dot{m}_{\mathrm{a}}^{p_{22}} + c_2 T_{\infty}^{p_{23}} + d_2 P_{\mathrm{spray}}^{p_{24}} + e_2, \tag{22b}$$

$$\mathrm{IPF} = a_3 \dot{m}_{\mathrm{w}}^{p_{31}} + b_3 \dot{m}_{\mathrm{a}}^{p_{32}} + c_3 T_{\infty}^{p_{33}} + d_3 P_{\mathrm{spray}}^{p_{34}} + e_3, \tag{22c}$$

where $\dot{m}_{\mathrm{w}}, P_{\mathrm{spray}}, \dot{m}_{\mathrm{a}}$, and T_{∞} refer to the water mass flow rate, spray pressure, air mass flow rate, and ambient temperature, respectively. The small letters (a - e, p) are regression coefficients and powers. It is noted that the cooling capacity can be directly computed from IPF using Eq. (18) thus, no additional correlation is proposed for the cooling capacity.

The operating parameters, their minimum and maximum values, and probability distributions are tabulated in Table 4. The data reported by Stachulak [10] is used in Table 4. Uniform distribution is assumed to generate random values for input variables as shown in the diagonal Kernel Density Estimate (KDE) plots for 1000 sample cases (Fig. 5). In Fig. 5, pressure levels are represented by different colors, with deeper hues denoting higher levels and paler hues indicating lower levels. Additionally, the pressure is a discrete variable in this analysis, since it has a specific set of discrete values.

3. Results and discussion

3.1. Model validation

For the numerical simulations of the work, mesh-independence studies were carried out to ensure the precision and robustness of the results. Parameters analyzed to ensure mesh independence include the grid size for the airflow CFD simulation, the number of droplet diameters, and the number of initial droplet velocity directions. For the size of the air flow simulation grid, a structured grid with 5×10^5 nodes was shown to be sufficient for the numerical simulation. For the number of droplet diameters and the number of initial droplet velocity directions, mesh independence studies indicate that 20 and 100 samples are enough, respectively. Figs. 6(a)–(c) illustrate the mesh-independent studies for the mentioned parameters.

The model is validated against experimental data of spray freezing reported in [10,34,35]. Table 5 represents the geometry and spray characteristics of the Frood Stobie mine [10] used in the model. The field data of the net heat rate and ice production from this mine is used for validation purposes in the present study. The net heat rate reported by Stachulak from the field data is 11.2 MW. Using Eqs. (12)–(14), under the conditions described in [10], a total heat rate of 12.4 MW

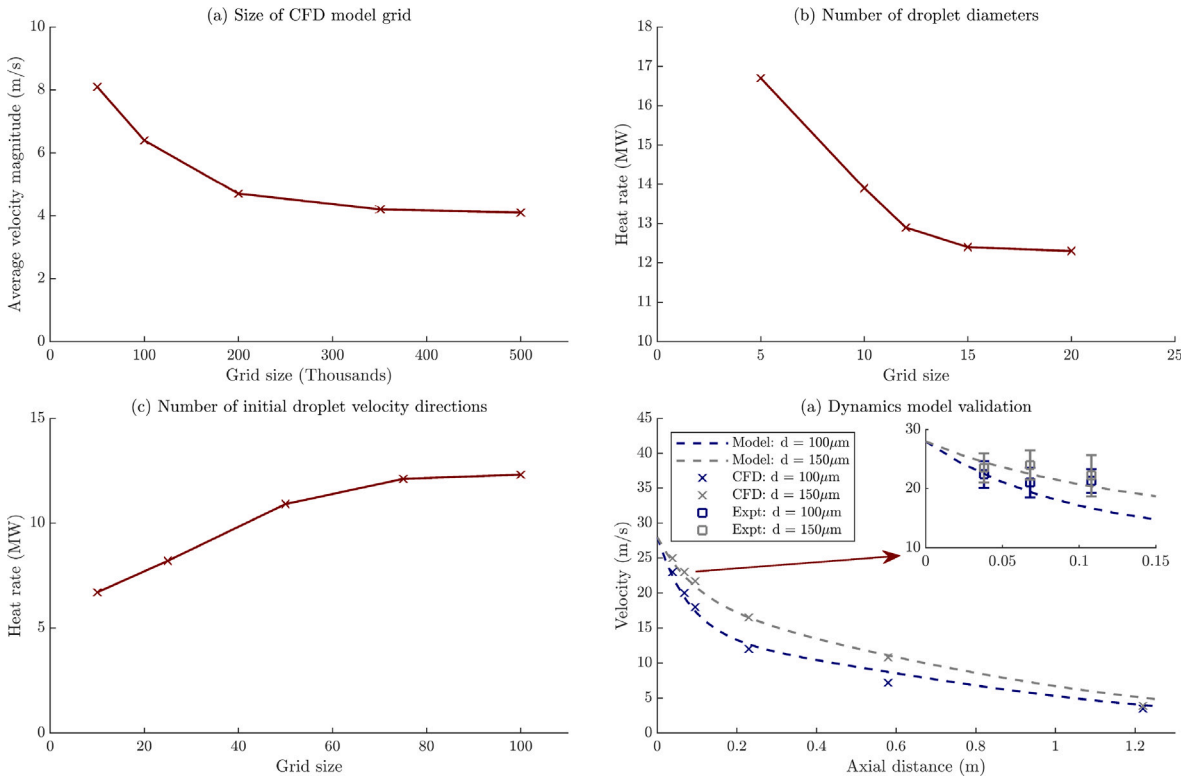

Fig. 6. Mesh-independent studies for (a) CFD model, (b) number of droplet diameters, and (c) number of initial droplet velocity directions. (d) Validation of the dynamics model using the data reported in [34,35].

Table 5
Stope properties used in the model.

Parameter	Value	Unit
Stope height	61	[m]
Stope length	61	[m]
Stope width	24.4	[m]
Spray shape	Flat spray	[–]
Spray size	0.75	[in]
Number of sprays	5	[–]
Orifice diameter of sprays	0.375	[in]

Table 6
Characteristics of the spray freezing setup described in [35].

Property	Value	Unit
Length of reactor	1.25	[m]
Diameter of reactor	0.8	[m]
Water flow rate	0.0125	[kg/s]
Gas velocity	0.9897	[m/s]
Water initial temperature	20	[°C]
Spray angle	30	[°]

is calculated using the developed model, which shows an acceptable relative error of $\frac{12.4-11.2}{11.2}\times 100 = 10.7\%$. Under the mentioned operating conditions, the total mass of ice formed in two stopes during the winter operations is 145,000 tons. Using our multiscale model, under a similar operating condition, the IPF comes out to be 85.3%. Considering the average flow rate of 18.9 kg/s and 1200 operating hours during the winter, the total mass of ice produced by two stopes is equal to,

$$m_{\text{ice}} = 2\times 0.853\times 18.9\left[\frac{\text{kg}}{\text{s}}\right]\times 1200\ [\text{h}]\times 3600\left[\frac{\text{s}}{\text{h}}\right]\times 0.001\left[\frac{\text{ton}}{\text{kg}}\right]$$
$$\approx 139{,}300\ [\text{ton}], \tag{23}$$

The relative error will be can be calculated as $\frac{145{,}000-139{,}300}{145{,}000}\times 100\% \approx 3.9$ which is acceptable. It is noticeable that a considerable amount of ice is produced during winter, which can provide a remarkable cooling capacity for summer season.

To illustrate the effectiveness of the developed framework in another application, we applied the model to the spray freezing setup described by Anandharamakrishnan [35] and Al-Hakim [34]. In the mentioned works, spray freezing is used as the first step of the spray freeze drying procedure. The setup consists of a cylindrical chamber with a hollow cone spray placed at the top of it. The characteristics of the setup are described in Table 6. The experimental results indicate that the outlet gas temperature at the center of the chamber is 250 K. The predicted outlet gas temperature from the model is 252.8 K, indicating a relative error equal to $\frac{|250-252.8|}{250}\times 100\% \approx 1.1$. It can be seen that the framework is capable of generating precise predictions of the spray freezing performance for a different application. The dynamics model is also validated using the experimental measurements of droplet velocity reported in [34] and CFD simulation of [35]. The velocity of droplets with sizes of 100 and 150 μm was measured at the center of the chamber and at three different axial distances from the nozzle, i.e., y = 0.038 m, 0.068 m, and 0.108 m. The absolute uncertainties for experimental values of d = 100 μm are 2.3, 2.5, and 2, while for d = 150 μm, they are 2.5, 2.5, and 3.5. It is observed from Fig. 6(d) that the model results are within the range of experimental values and agree well with the CFD simulations.

The results of the parametric study are discussed in this part, highlighting the relationships between the input and output parameters. As discussed before, the net heat rate, cooling capacity, outlet air temperature, and ice packing fraction (IPF) are the monitored variables that indicate the performance of the spray freezing for heating and cooling in cold-region mines. As mentioned before, the parametric study was conducted using four different sample sizes — 100, 200, 500, and 1000 cases — to ensure the results are independent of sample size. The probability distribution functions are illustrated in Fig. 7. It is observed that the results stabilize after 500 samples, thus the case of 1000 sample was selected for the regression analysis.

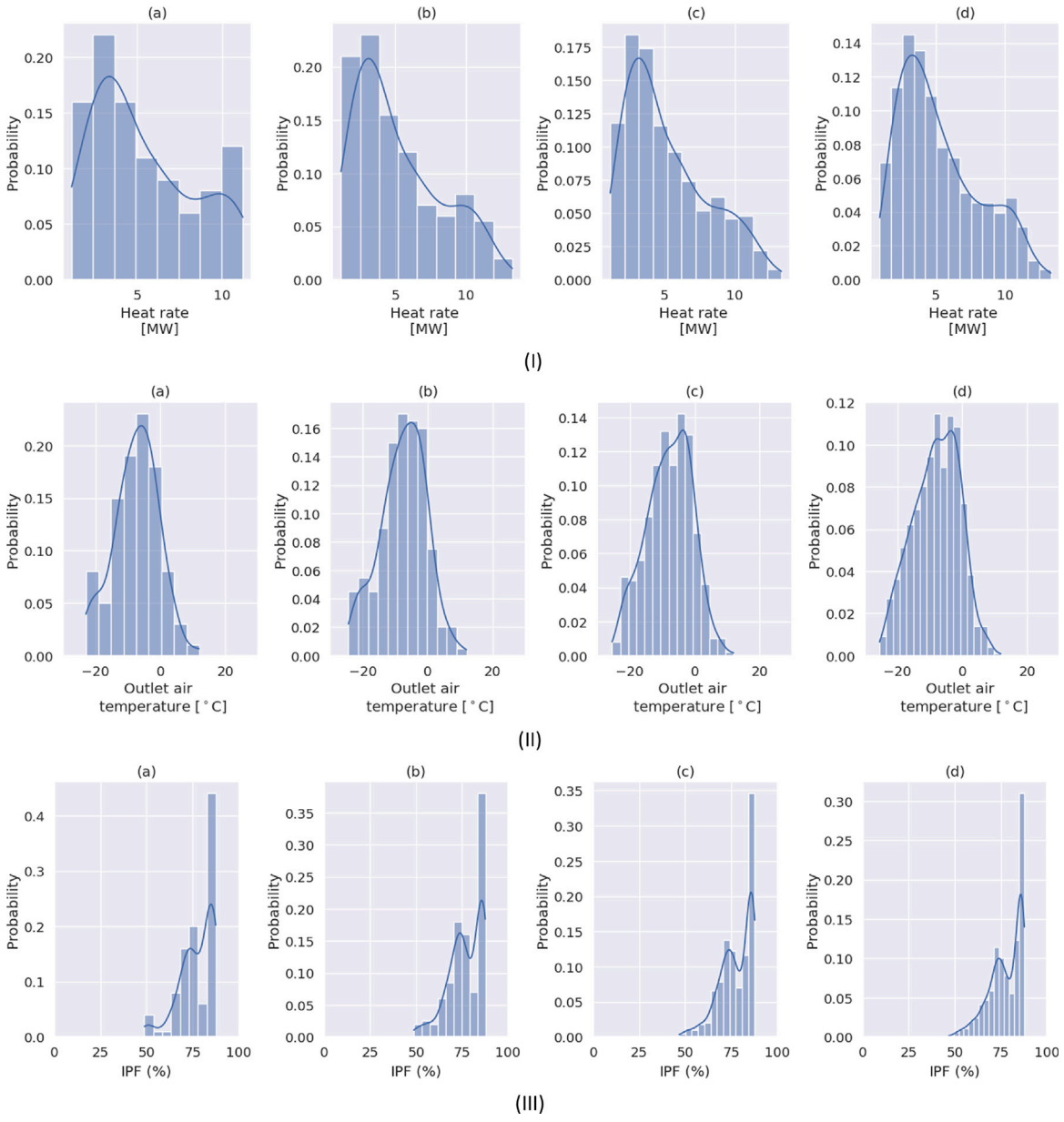

Fig. 7. The probability distribution of (I) net heat rate, (II) outlet air temperature, and (III) IPF considering (a) 100, (b) 200, (c) 500, and (d) 1000 simulation cases.

Table 7
Regression coefficients in Eqs. (22a) and (22b) and corresponding R^2 values for the case of 1000 samples.

Regression coefficients	Heat rate [MW]	Outlet air temperature [°C]	Ice packing fraction [%]
	i = 1	i = 2	i = 3
a_i	2.73×10^{-1}	4.04×10^{-1}	-3.65×10^{-2}
b_i	4.84×10^{-1}	6.66	2.28
c_i	-2.38×10^{-1}	6.75×10^{-1}	−1.00
d_i	-2.22×10^{-1}	-2.90×10^{-1}	−1.54
e_i	−4.06	-1.14×10^{1}	6.14×10^{1}
$[p_{i,1}, p_{i,2}, p_{i,3}, p_{i,4}]$	[1, 1, 1, 1]	[1, −1, 1, 1]	[1, 1, 1, 1]
R^2	0.92	0.92	0.90

3.2. The net heat rate

The effects of random combinations of operating variables are evaluated on the heat rate in this part. The probability distribution of the heat rate for the sample sizes of 100, 200, 500, and 1000 is shown in Fig. 7(I). It can be seen that the heat rate distribution follows a multi-modal behavior. To determine the coefficients of Eq. (22a), a regression analysis is performed, and the results are shown in Table 7, yielding an easy-to-compute correlation for determining the heat rate (in megawatts) as below

$$\dot{Q}_h = (2.73 \times 10^{-1})\dot{m}_w + (4.84 \times 10^{-1})\dot{m}_a - (2.38 \times 10^{-1})T_\infty - (2.22 \times 10^{-1})P_{spray} - 4.06. \quad (24)$$

Here $\dot{m}_a$ is the air flow rate [MCFM], $\dot{m}_w$ is the water flow rate [kg/s], T_∞ is the ambient temperature [°C], and P_{spray} is the spray pressure. The spray pressure in Eq. (24) takes three values of 0, 1, and 2 representing 60, 70, and 80 bars, respectively.

The effects of input variables on the heat rate are plotted in Fig. 8, with the pressure levels represented by colors; darker shades indicate higher pressure levels. It can be inferred from this figure that the heat rate is primary affected by the water flow rate and ambient temperature, as compared to the air flow rate or spray pressure. This is because the heat rate is largely determined by the latent heat of freezing,

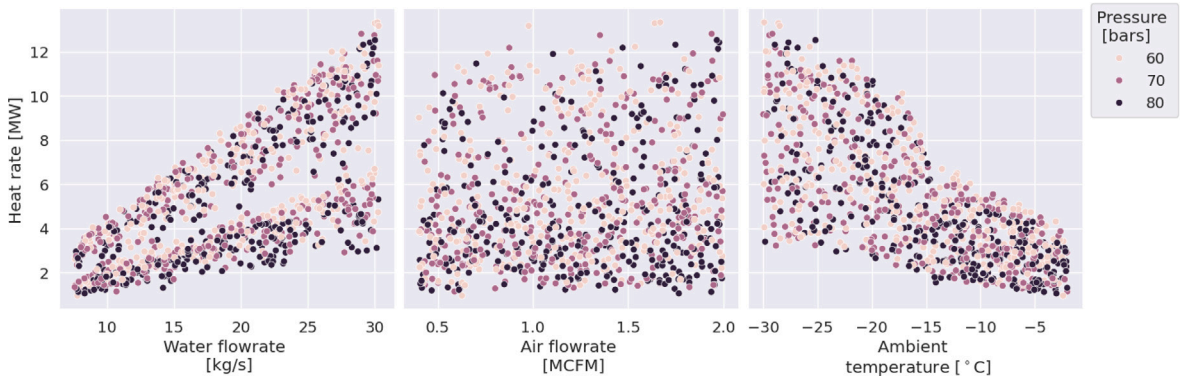

Fig. 8. The effects of operating parameters on the net heat rate for 1000 simulation cases.

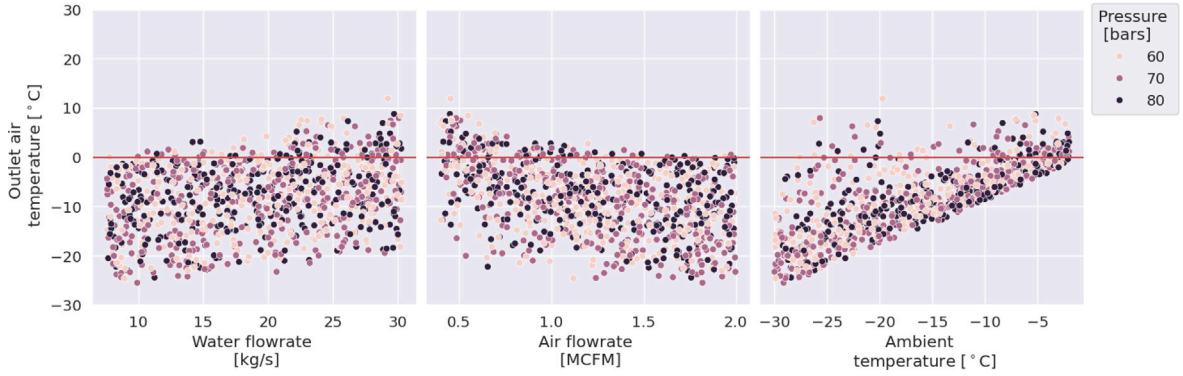

Fig. 9. The effects of operating parameters on the outlet air temperature for 1000 simulation cases.

which depends directly on the mass of frozen water. Also, the ambient temperature not only affects the freezing time of droplets, but also determines whether the supercooling stage occurs during the freezing. It can be seen that when the ambient temperature is approximately above −15 °C, the heat rate is considerably lower compared to cases where the ambient temperature is below −15 °C. This phenomenon can be attributed to different freezing scenarios for the mentioned temperature ranges, i.e., freezing without supercooling and freezing with supercooling. This difference is also observed in the graph showing heat rate versus water flow rate, as there are two distinct areas which correspond to two different freezing types. It is noteworthy that the water nucleation temperature is around −15 °C. Surprisingly, the effects of air flow rate and spray pressure on the heat rate do not follow a clear trend, reaffirming the significant effects of water flow rate and ambient temperature on heat rate. In general, a higher heat rate is desirable as it results in a higher outlet air temperature and ice production, which in turn leads to a higher cooling capacity. As stated at the beginning of this section, the heat rate calculated from the model for the case of Frood-Stobie mine using the data given in [10], is 12.4 MW which is equivalent to 650 MJ/m^3 considering the average flow rate of 18.9 kg/s. It is a smaller heat rate as compared to fuels such as Propane which produces around 91,500 BTUs per gallons energy [36] (i.e., around 25,500 MJ/m^3). However, the spray freezing is cheaper in terms of operating costs, and also it is less pollutant. Moreover, the ice produced during the process not only can be used for cooling, but it can be pumped back to the system after being melted [37].

3.3. Outlet air temperature

It is crucial to keep the air temperature of the stope above the freezing point of water, preventing the infrastructure from freezing. To compute the air temperature, Eq. (15) is used. For thermophysical properties, temperature-dependent values are used in the model, which are taken from Akhtar et al. [38]. The probability distribution of the outlet air temperature for different number of sample sizes is shown in Fig. 7(II). From this figure, it can be deduced that the outlet air temperature follows a Gaussian distribution with a mean around −10 °C. The following expression is developed using the linear regression analysis to calculate the outlet air temperature in Centigrade

$$T_{a,out} = (4.04\times10^{-1})\dot{m}_w + (6.66)\dot{m}_a^{-1} + (6.75\times10^{-1})T_\infty - (2.90\times10^{1})P_{spray} - 1.14\times10^{1}. \quad (25)$$

Fig. 9 depicts the effects of water flow rate, spray pressure, air flow rate, and ambient air temperature on the outlet air temperature. As it can be observed, the outlet air temperature is a strong function of the ambient temperature. The freezing temperature of water is shown with a red line in this Figure. It can be observed that when higher water flow rate are injected, it is more probable to keep the air temperature above the freezing point of water. Additionally, a lower ambient temperature makes it more difficult to raise the outlet air temperature above 273.15 K. Lastly, the air flow rate and spray pressure have weak influence on the outlet air temperature.

The results shown in Fig. 9 will be of considerable interest to engineers. Once the outlet air temperature is above 0 °C, usually no heating from fuels such as Propane is required. However, for the case that the outlet air temperature calculated from Eq. (25) is below 0 °C, heating from fuels is still needed to increase the air temperature to above 0 °C.

3.4. IPF and cooling capacity

In the air heating of mine ventilation systems using spray freezing, high values of ice packing fraction (IPF) are desirable to maximize air heating and generate more ice for cooling to reduce fuel costs

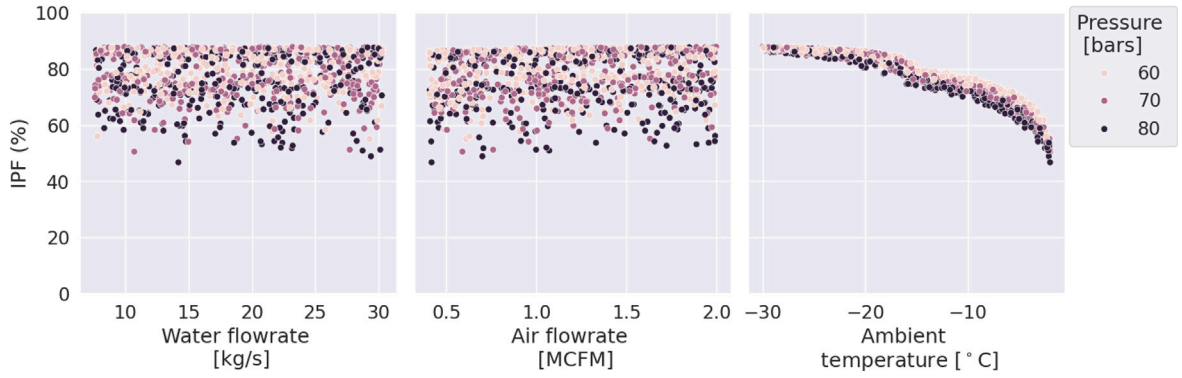

Fig. 10. The effects of different operating parameters on the ice packing fraction (IPF) for 1000 simulation cases.

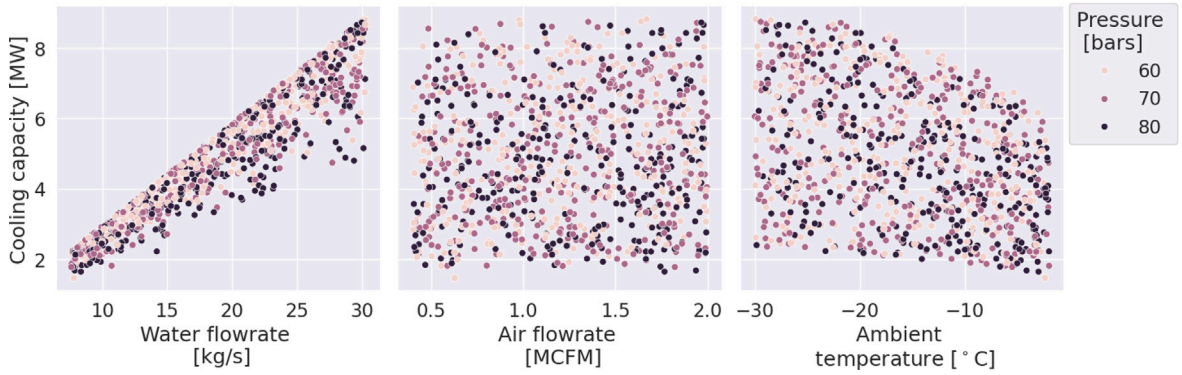

Fig. 11. The effects of different operating parameters on the cooling capacity for 1000 simulation cases.

and emissions. Ice storage capacity of a mine should be considered in designing spray freezing setups due to space constraints. Also, a large amount of ice accumulation at the stope bottom will decrease IPF over time because of a decrease in the residence time of droplets. Therefore, IPF is a decisive factor to be considered in designing spray freezing setups for mines. Using the regression analysis, the following correlation is obtained for IPF (in %)

$$\mathrm{IPF} = (-3.65\times10^{-2})\dot{m}_{\mathrm{w}} + 2.28\dot{m}_{\mathrm{a}} - T_{\infty} - 1.54P_{\mathrm{spray}} + 6.14\times10^{1}. \quad (26)$$

The correlation outlined in Eqs. (24), (25), and (26) provide a straightforward method to estimate the performance of the spray freezing system under a specific condition. Fig. 10 illustrates the variations of IPF with changes in input variables. It is observed that the IPF is mostly dependent on the ambient temperature. This is due to the fact that the ambient temperature determines the freezing time of droplets, which in turn affects the IPF. Similar to the case of heat rate, for ambient temperatures approximately above −15 °C, the IPF is remarkably lower compared to the cases where the ambient temperature is below −15 °C. Again, this stems from the longer freezing times and different freezing scenarios for ambient temperatures below or above the water nucleation temperature. In most cases, the IPF is above 50% due to the large stope size in Frood-Stobie mine ($61\times61\times24.4$ m^3). It is also noticeable that the IPF has a weak dependency on the water and air flow rates and the spray pressure. Fig. 7(III) depicts the probability distribution of IPF values for different simulation sizes. A multi-modal distribution can be observed (centered around 70 and 90 percent) which reaffirms the notion that high IPF values depend on the freezing type. The cooling capacity is calculated using Eq. (18). Fig. 11 indicates the effects of each input parameter on the cooling capacity. As expected, the cooling capacity is mostly dependent on the water flow rate and ambient temperature, which can also be inferred from Eq. (18).

The results indicate that the developed model has the capability to evaluate the performance of the spray freezing for mine heating and cooling under various operating conditions. The model can be easily adjusted to be applied to real-world mines under various stope geometries, spray characteristics, water and air flow rates, and ambient temperatures. Compared to the existing models based on CFD calculations, the current framework can generate results in a quick manner while maintaining an acceptable accuracy. The model, however, does not compute the air temperature profile and the effects of spray dynamics on the air flow, limiting its capability to provide precise local insights on the air thermo-hydraulic profiles.

4. Conclusion

The spray freezing system, as an innovative solution to address the heating and cooling needs of mines, was studied in this work. A high-resolution framework to compute the performance of spray freezing is developed, incorporating models of droplet freezing, spray-droplet dynamics, and air flow inside the stope. The modeling results can predict the heat rate and ice packing fraction (IPF) of the spray freezing system to within 10% and 5% values of the field data, respectively. The modeling results were subsequently used to conduct a parametric study, analyzing the effects of operating variables on the system efficiency. Three easy-to-use correlations were developed to compute the heat rate, outlet air temperature, and IPF of the setup for different sets of input variables. These correlations enable engineers to evaluate the effectiveness of the spray freezing system quickly, leading to a more straight-forward design procedure. Key results of the parametric study can be summarized as below:

- The dominant freezing type when the ambient temperature is approximately above −15 °C is freezing without supercooling. However, when the ambient temperature is below −15 °C, most droplets experience supercooling.

- The ambient temperature and water flow rate significantly influence the heat rate and cooling capacity of the spray freezing process.
- The outlet air temperature is controlled primarily by the ambient air temperature the most as compared to the water and air flow rates and nozzle pressure.
- The IPF value is mostly dependent on the ambient temperature and shows a multi-modal behavior due to different freezing mechanisms based on the ambient temperature.

Future works include:

- Studying the influence of droplets on the air flow and incorporating the spatial distributions of the air temperature and velocity into the model,
- Studying the effects of the ice accumulation on the droplets' residence times, and
- Analyzing the effects of spray break-up, angle, and distance on the model results.

CRediT authorship contribution statement

Mohammaderfan Mohit: Writing – original draft, Visualization, Validation, Supervision, Software, Methodology, Investigation, Conceptualization. **Saad Akhtar:** Writing – original draft, Visualization, Validation, Software, Methodology, Investigation, Conceptualization. **Minghan Xu:** Writing – review & editing, Visualization, Validation, Software, Methodology, Investigation, Conceptualization. **Agus P. Sasmito:** Writing – review & editing, Supervision, Resources, Project administration, Investigation, Funding acquisition, Conceptualization.

Declaration of competing interest

The authors declare that they have no known competing financial interests or personal relationships that could have appeared to influence the work reported in this paper.

Acknowledgments

A.P.S., M.X., and M.M. acknowledged the funding from Natural Sciences and Engineering Research Council of Canada, Canada (NSERC RGPIN-2021-02901) and Fonds de Recherce du Quebec (FRQ-NT-PR-300597).

Data availability

Data will be made available on request.

References

[1] P. Guo, M. He, L. Zheng, N. Zhang, A geothermal recycling system for cooling and heating in deep mines, Appl. Therm. Eng. 116 (2017) 833–839.
[2] S. Akhtar, A. Madiseh, A. Sasmito, Numerical investigation of a novel phase-change renewable energy system for underground mine heating and cooling, in: Refrigeration Science and Technology, 2018-May, 2018.
[3] S.A. Ghoreishi-Madiseh, A.P. Sasmito, F.P. Hassani, L. Amiri, Heat transfer analysis of large scale seasonal thermal energy storage for underground mine ventilation, Energy Procedia 75 (2015) 2093–2098.
[4] A.P. Sasmito, J.C. Kurnia, E. Birgersson, A.S. Mujumdar, Computational evaluation of thermal management strategies in an underground mine, Appl. Therm. Eng. 90 (2015) 1144–1150.
[5] F. Mercier-Langevin, Laronde extension–mine design at three kilometres, Min. Technol. 120 (2) (2011) 95–104.
[6] D.X. Wilson, Heat loads and cooling at laronde, in: CIM Montreal 2015, 2015.
[7] A.F. Kuyuk, S.A. Ghoreishi-Madiseh, F.P. Hassani, A.P. Sasmito, L. Amiri, J. Templeton, Performance and economic assessment of large-scale deep-lake cooling systems: A Canadian example, Energy Procedia 158 (2019) 43–48.
[8] Y. Xu, Z. Li, Y. Chen, M. Jia, M. Zhang, R. Li, Synergetic mining of geothermal energy in deep mines: An innovative method for heat hazard control, Appl. Therm. Eng. 210 (2022) 118398.
[9] Y. Gao, Y. Ning, C. Wu, M. Xu, S. Akhtar, A.S. Mujumdar, A.P. Sasmito, Experimental investigation of producing ice slurry with water using opposed-nozzle impinging jet method, Appl. Therm. Eng. 219 (2023) 119568.
[10] J. Stachulak, Ventilation strategy and unique air conditioning at inco limited, CIM Bull. (Can. Inst. Min. Metall.) (Canada) 84 (950) (1991).
[11] A. Dehghani-Sanij, S. MacLachlan, G. Naterer, Y. Muzychka, R. Haynes, V. Enjilela, Multistage cooling and freezing of a saline spherical water droplet, Int. J. Therm. Sci. 147 (2020) 106095.
[12] K. Shi, J. Huang, X. Duan, An analytical framework for predicting the total freezing delay time of water droplet impact on hydrophobic solid surfaces, Int. J. Therm. Sci. 196 (2024) 108726.
[13] S. Akhtar, M. Xu, M. Mohit, A.P. Sasmito, A comprehensive review of modeling water solidification for droplet freezing applications, Renew. Sustain. Energy Rev. 188 (2023) 113768.
[14] M. Xu, S. Akhtar, M. Mohit, A.F. Zueter, A.P. Sasmito, Asymptotic analysis of a two-phase stefan problem in an annulus with the convective boundary, Int. J. Therm. Sci. 196 (2024) 108744.
[15] M. Calvo-Schwarzwälder, T.G. Myers, M.G. Hennessy, The one-dimensional stefan problem with non-Fourier heat conduction, Int. J. Therm. Sci. 150 (2020) 106210.
[16] S. Akhtar, M. Xu, A.P. Sasmito, Development and validation of an asymptotic solution for a two-phase stefan problem in a droplet subjected to convective boundary condition, Int. J. Therm. Sci. 164 (2021) 106923.
[17] J.P. Hindmarsh, A.B. Russell, X.D. Chen, Experimental and numerical analysis of the temperature transition of a suspended freezing water droplet, Int. J. Heat Mass Transfer 46 (7) (2003) 1199–1213.
[18] B. Zhang, S. Zhong, Y. Cao, H. Zhang, L. Chen, J. Wei, Freezing of sessile water droplets on titanium alloy surfaces with various roughness: An in-situ experimental study, Int. J. Therm. Sci. 203 (2024) 109099.
[19] C. Chen, Z. Jing, C. Feng, X. Zou, M. Qiao, D. Xu, S. Wang, Two-phase flow and morphology of the gas–liquid interface for bubbles or droplets in different microchannels, Phys. Fluids 35 (9) (2023).
[20] B. Jalili, P. Jalili, Numerical analysis of airflow turbulence intensity effect on liquid jet trajectory and breakup in two-phase cross flow, Alex. Eng. J. 68 (2023) 577–585.
[21] N. Ashgriz, Handbook of Atomization and Sprays: Theory and Applications, Springer Science & Business Media, 2011.
[22] Z. Gao, Y. Liu, G. Liu, Q. Zhang, Y. Deng, Effect of crossflow temperature on liquid column trajectory, Appl. Therm. Eng. (2024) 123303.
[23] H. Zhang, H. Zhang, B. Bai, Numerical study on flow structures of a hollow cone spray in crossflow, Heat Transf. Eng. 43 (8–10) (2022) 737–753.
[24] A.H. Lefebvre, V.G. McDonell, Atomization and Sprays, CRC Press, 2017.
[25] M. Mohit, M. Xu, J.C. Kurnia, A.S. Mujumdar, A.P. Sasmito, Spray freezing: An overview of applications and modeling, Drying Technol. (2024) 1–19.
[26] C. Anandharamakrishnan, J. Gimbun, A. Stapley, C.D. Rielly, Application of computational fluid dynamics (CFD) simulations to spray-freezing operations, Drying Technol. 28 (1) (2009) 94–102.
[27] J. Hindmarsh, A. Russell, X. Chen, Fundamentals of the spray freezing of foods—microstructure of frozen droplets, J. Food Eng. 78 (1) (2007) 136–150.
[28] I.B. Sebastião, B. Bhatnagar, S. Tchessalov, A kinetic model for spray-freezing of pharmaceuticals, J. Pharm. Sci. 110 (5) (2021) 2047–2062.
[29] K. Trapani, Techno-economic of an ice stope thermal storage for mine heating and cooling in sub-arctic climates, in: Proceedings of 17th North American Mine Ventilation Symposium, 2019, pp. 709–715.
[30] M. Xu, Y. Gao, F. Fang, S. Akhtar, B.A. Chaedir, A.P. Sasmito, Experimental and unified mathematical frameworks of water-ice phase change for cold thermal energy storage, Int. J. Heat Mass Transfer 187 (2022) 122536.
[31] S. Akhtar, M. Xu, A.P. Sasmito, A novel crystal growth model with nonlinear interface kinetics and curvature effects: Sensitivity analysis and optimization, Cryst. Growth Des. 21 (6) (2021) 3251–3265.
[32] S. Akhtar, M. Xu, A.P. Sasmito, Development and validation of a semi-analytical framework for droplet freezing with heterogeneous nucleation and non-linear interface kinetics, Int. J. Heat Mass Transfer (2020) 120734.
[33] P.E. Santangelo, Characterization of high-pressure water-mist sprays: Experimental analysis of droplet size and dispersion, Exp. Therm Fluid Sci. 34 (8) (2010) 1353–1366.
[34] K. Al-Hakim, An Investigation of Spray-Freezing and Spray-Freeze-Dryings (Ph.D. thesis), Loughborough University, 2004.
[35] C. Anandharamakrishnan, Experimental and Computational Fluid Dynamics Studies on Spray-Freeze-Drying and Spray-Drying of Proteins (Ph.D. thesis), Loughborough University, 2008.
[36] C.F. Brasington, Utility Usage in Small Slaughter Plants, Vol. 174, Department of Agriculture, Agricultural Research Service, Southern Region, 1978.
[37] Y. Gao, M. Mohit, J. Luo, M. Xu, F. Fang, A.S. Mujumdar, A.P. Sasmito, Development of a novel continuous nanofluid ice slurry generator: Experimental and theoretical studies, Appl. Therm. Eng. (2024) 122667.
[38] S. Akhtar, M. Xu, A.P. Sasmito, Development and validation of an asymptotic solution for a two-phase stefan problem in a droplet subjected to convective boundary condition, Int. J. Therm. Sci. 164 (2021) 106923.